Accretion of Intergalactic Matter onto S-galaxies: Formation Mechanisms of Polar Rings

Sergei Khrapov,

Alexander Khoperskov, Nikita Khrapov

Volgograd State University (VolSU)

Polar Rings in Galaxies

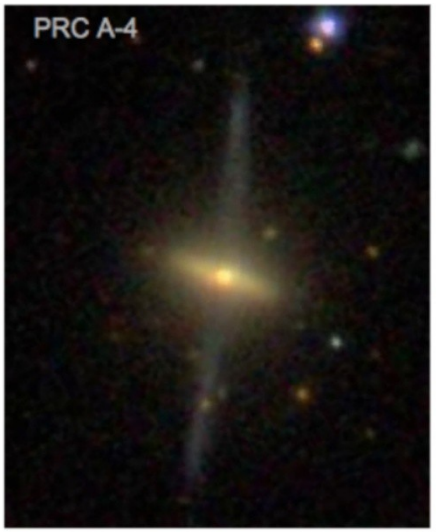

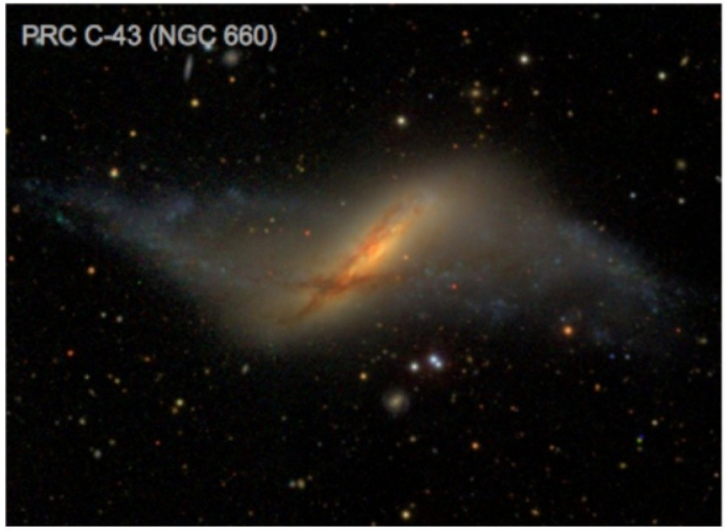

Polar Ring Catalog (PRC, Whitmore et al.)

Deg et al. 2023, MNRAS

Astrophysical Research Instruments

Observational Data

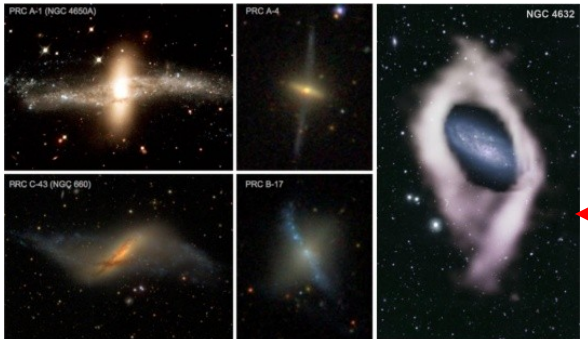

Theoretical Models

Galactic Components:

- ✓ Dark Matter (Halo, Filaments,...)
- ✓ Stars (Disk, Bulge, Halo, Ring)
- ✓ Gas (Disk, Jet, Halo, Ring)

Numerical Models:

- ✓ N-body Methods (PP, TreeCod)
- ✓ Gas Dynamics Methods (SPH, TVD)
- ✓ Heating and Cooling
- ✓ Chemical Kinetics
- ✓ Feedback (Gas ↔ Stars)

Verification and Calibration of Model Parameters

Supercomputer Simulations

GPU – clusters:

- ✓ MSU Supercomputer Lomonosov-2 (68 x Nvidia Tesla V100, 476 TFlop/s)
- ✓ VolSU Supercomputer DGX-1 (8 x Nvidia Tesla V100)

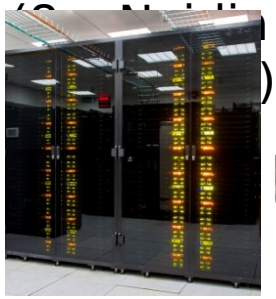

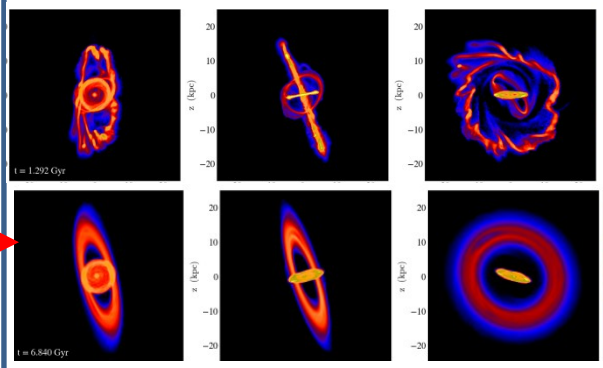

Supercomputer Simulations I

Monthly Notices
of the
ROYAL ASTRONOMICAL SOCIETY

MNRAS **500,** 3870–3888 (2021)
Advance Access publication 2020 October 27

doi:10.1093/mnras/staa3330

Extreme kinematic misalignment in IllustrisTNG galaxies: the origin, structure, and internal dynamics of galaxies with a large-scale counterrotation

Sergey Khoperskov,[1,2,3★] Igor Zinchenko,[4,5] Branislav Avramov,[6] Sergey Khrapov,[7]
Peter Berczik,[5,6,8] Anna Saburova,[1,9] Marina Ishchenko,[5] Alexander Khoperskov,[7]
Claudia Pulsoni,[3,10] Yulia Venichenko,[11] Dmitry Bizyaev[9,12] and Alexei Moiseev[13]

ABSTRACT

We provide an in-deep analysis of 25 galaxies with substantial counterrotation from IllustrisTNG100 simulations in the stellar mass range $2\times10^9-3\times10^{10}\,M_\odot$. The counterrotation is a result of an external gas infall ≈2–8 Gyr ago. The infall leads to the removal of pre-existing gas, which is captured and mixed together with the infalling component. This mixture ends up in the counterrotating gaseous disc where ≈90 per cent of counterrotating stars formed in-situ. During the early phases of the infall, gas can be found in extended structures which, in some galaxies, are similar to (nearly-) polar ring-like components. We suggest that the AGN activity does not cause the counterrotation, although it is efficiently triggered by the retrograde gas infall, and it correlates well with the misaligned component appearance. We also find the vertical-to-radial velocity dispersion ratio above unity implying the importance of misalignment in shaping the velocity ellipsoids.

Key words: galaxies: evolution – galaxies: formation – galaxies: interactions – galaxies: kinematics and dynamics – galaxies: structure.

The Gaseous Disc Replacement via a Retrograde Accretion

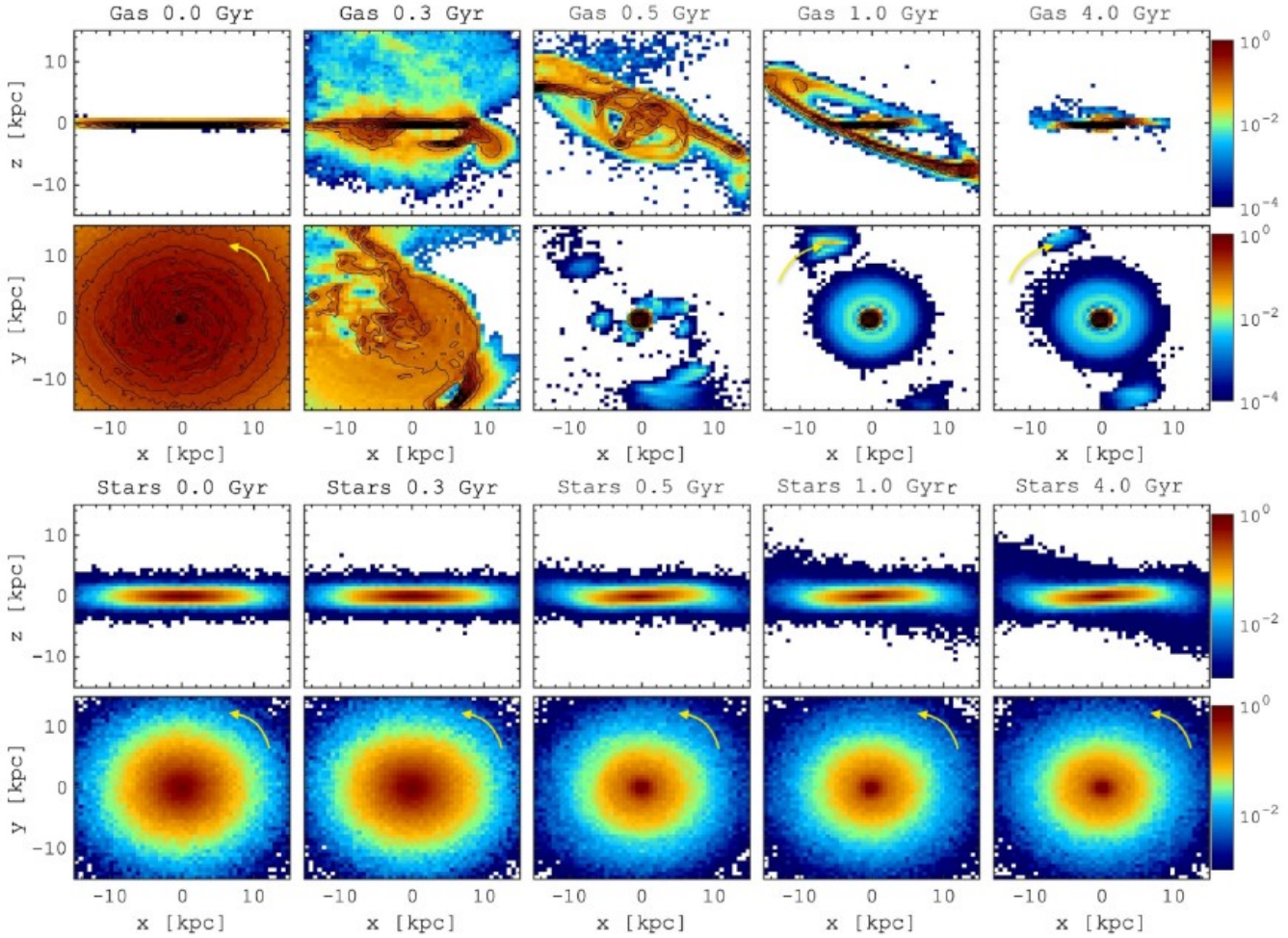

Figure 16. Evolution of gas (top frames) and stars (bottom frames) in a simulation of a retrograde gas infall on to a gas-rich galaxy. For th ein-plane (XY) maps we show only particles with $|z| < 1$ kpc. The gas distribution maps include the gas with a temperature of $<20\,000$ K. The galactic plane is always aligned with the XY-plane. The initial gaseous disc is kicked-out from the galactic plane (stars) by the infalling gas, with almost a lack of gas in the disc plane at $\approx$0.5. Once the gas settles back to the galactic plane, it inherits the direction of its rotation from the infalling gas. The stellar disc shrinks towards the centre, but remains mostly unperturbed. The yellow arrows indicate the direction of rotation of gas and stars.

Feeding the Galaxies: Retrograde Versus Prograde Gas Infall

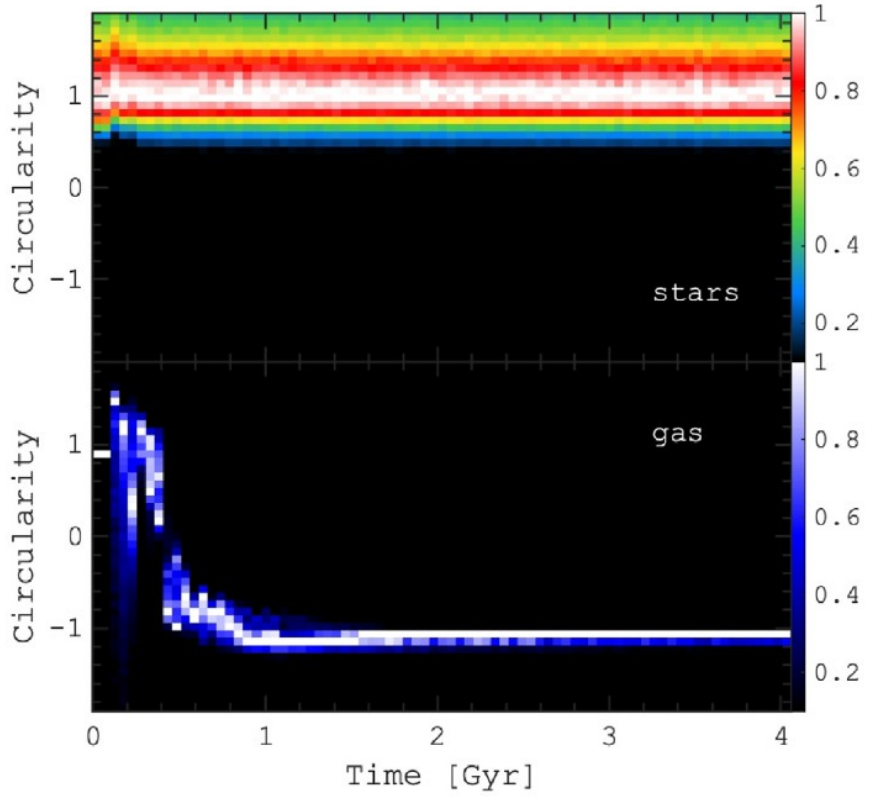

Figure 17. Evolution of the circularity distribution for stars (top) and gas (bottom) in a toy model of the retrograde gas infall on to a gas-rich galaxy, similar to Fig. 4 for the IllustrisTNG galaxies.

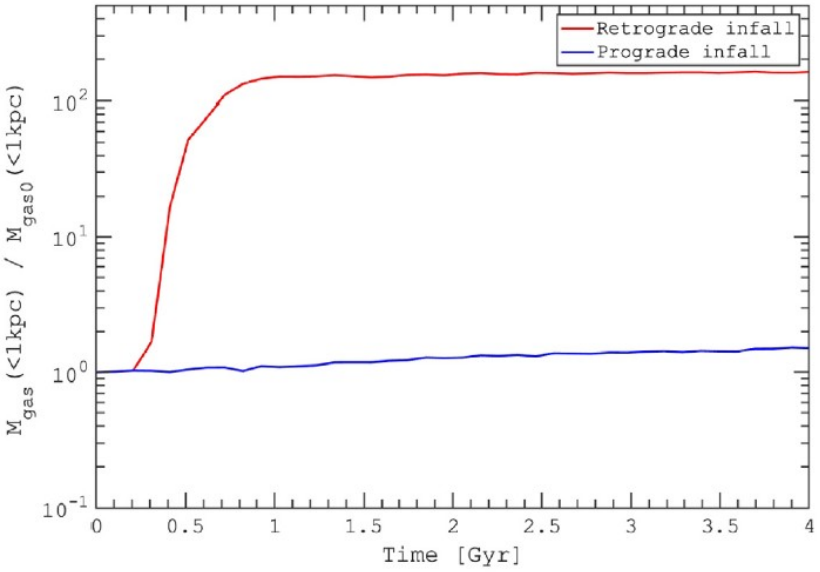

Figure 18. The gas mass in the central kpc in two toy models of the retrograde (red) and prograde (blue) gas infall to the gas-rich galaxy. During the retrograde accretion the gas efficiently falls into the galactic centre and is able to stimulate the activity of a central black hole.

Supercomputer Simulations II

 Published by De Gruyter Open Access March 8, 2024

Retrograde infall of the intergalactic gas onto S-galaxy and activity of galactic nuclei

Sergey S. Khrapov and Alexander V. Khoperskov

From the journal Open Astronomy
https://doi.org/10.1515/astro-2022-0231

Abstract

We present the results of numerical simulations focused on the accretion of intergalactic gas onto a gas-rich S-type disc galaxy. Our investigation explores the conditions favouring the emergence of counterrotating stellar and gaseous components within the galaxy, leading to the inflow of gas towards the central kiloparsec of the galaxy. Notably, we find that the most substantial reservoir of gas, serving as fuel for galactic nucleus activity, resides within the central region during the retrograde infall of gas at an incident angle of approximately 20° relative to the galactic plane. Departures from this angle significantly diminish the gas flow rate towards the galactic centre. Conversely, the prograde infall of intergalactic gas makes a marginal contribution to the gas content in the central region and cannot supply fuel to the active galactic nucleus. An intriguing characteristic of the observed retrograde impact is the emergence of a rotating polar ring at the galaxy's periphery, primarily originating from intergalactic gas.

Keywords: galaxies; gas accretion; counterrotation; numerical simulation

Model and Initial Setup

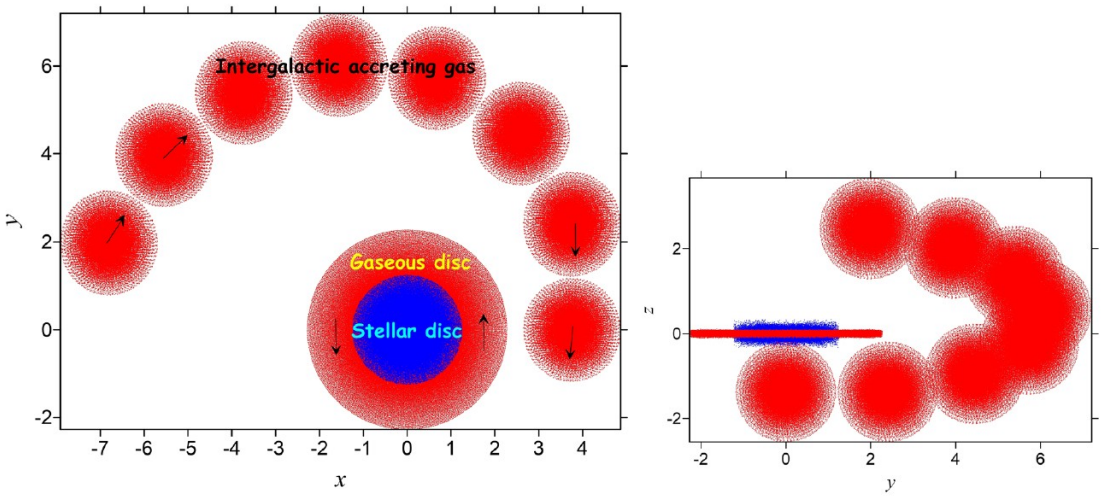

Figure 1: Scheme of intergalactic gas infall onto S-galaxy in computational experiments.

The parameters of the galactic components in the basic model are listed below:

- the stellar disc with optical radius $R_{\rm opt} = 10$ kpc, the total mass $M_* = 4 \times 10^{10} M_\odot$, and the radial scale length $r_d = 2.5$ kpc;
- the gas disc with size $R_g = 20$ kpc and the total mass $M_g = 0.8 \times 10^{10} M_\odot$;
- the dark matter halo with the mass inside of the optical radius $M_h = 20 \times 10^{10} M_\odot$ and the radial scale length $a = 2.5$ kpc;
- the spheroidal clumps of intergalactic gas ($J = 1, 2, \ldots, 8$) with a single cloud mass of $M_J = 0.2 \times 10^{10} M_\odot$, radius $R_J \approx 5$ kpc, and the total gas mass $8M_J$.

The equations of motion of gravitationally interacting gaseous and collisionless particles have the following form:

$$\frac{{\rm d}^2 \mathbf{r}_i}{{\rm d}t^2} = \begin{cases} -\dfrac{\nabla p_i}{\varrho_i} + \mathbf{f}_i^h + \displaystyle\sum_{j=1, j\neq i}^{N} \mathbf{f}_{ij}, & 0 \le i < N_g, \\ \mathbf{f}_i^h + \displaystyle\sum_{j=1, j\neq i}^{N} \mathbf{f}_{ij}, & Ng \le i < N = Ng + N_*, \end{cases} \tag{1}$$

where the radius vector $\mathbf{r}_i(t) = \int \mathbf{v}_i {\rm d}t$ determines the position of the ith particle in space, $\mathbf{v}_i$ is the velocity of the ith particle, and ϱ_i and p_i are the volume density and gas

$$\mathbf{f}_{ij} = -G \frac{m_j (\mathbf{r}_i - \mathbf{r}_j)}{[(\mathbf{r}_i - \mathbf{r}_j)^2 + \delta^2]^{3/2}}, \tag{2}$$

where G is the gravitational constant, m_j is the mass of the jth particle, and δ is the gravitational smoothing length at very short distances. The length δ for all components is the same and amounts to $\delta = 20$ pc.

The gas dynamics model also includes the equation of state of the gas $e = e(p, \varrho)$ and the conservation equation of specific internal energy e_i in the following form:

$$\frac{{\rm d}e_i}{{\rm d}t} = -\frac{p_i}{\varrho_i} \nabla \cdot \mathbf{v}_i + Q - \Lambda, \tag{3}$$

$$e_i = \frac{p_i}{(\gamma - 1)\varrho_i}, \tag{4}$$

where γ is the adiabatic index, and Q and Λ are the heating and cooling functions, respectively.

This gives the following conversion factors from dimensionless units in the numerical model into the physical units:

$$\ell_m = 4 \times 10^{10} M_\odot, \quad \ell_r = 10 \text{ kpc},$$
$$\ell_v \approx 131.5 \text{ km s}^{-1}, \quad \ell_t \approx 76 \times 10^6 \text{ years}.$$

Simulation Results: Collision Dynamics

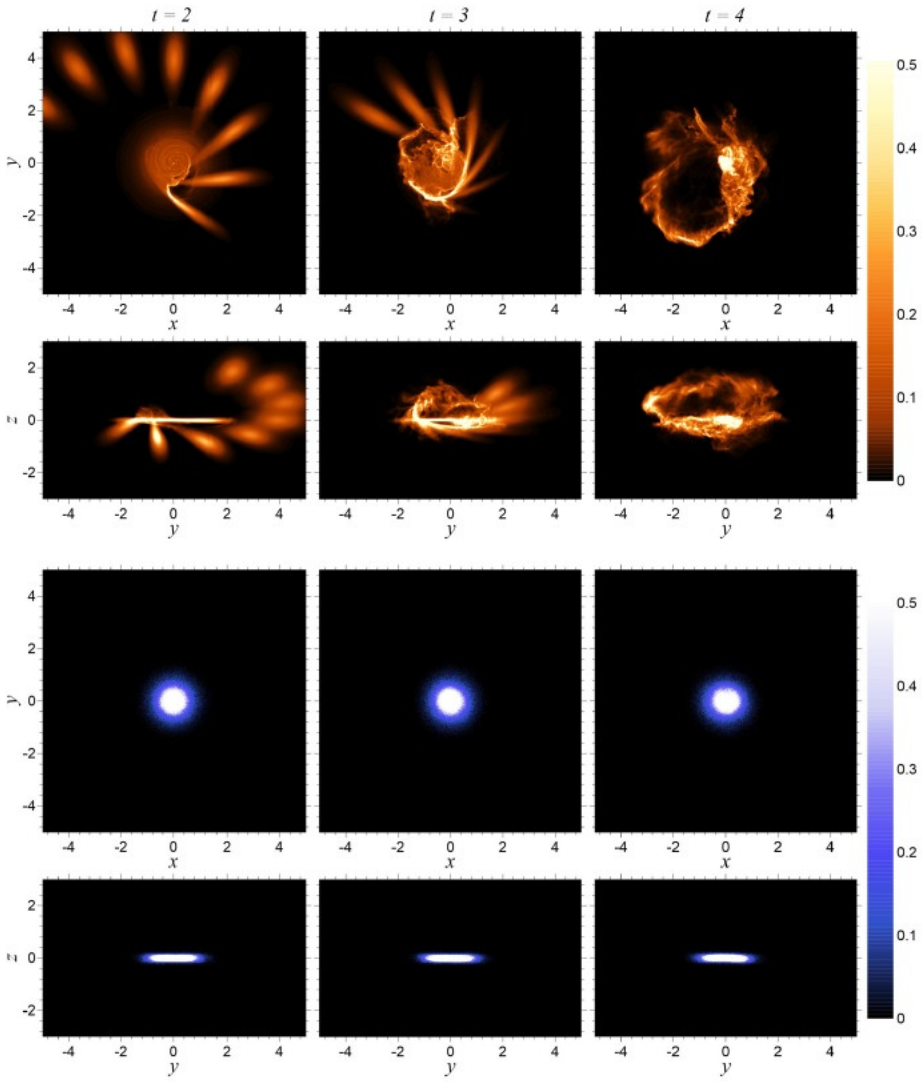

Figure 2: Surface density distributions of the gaseous (orange colour at the top) and stellar (blue colour at the bottom) components in various projections (XY and YZ) at the initial stages of collision of retrograde intergalactic gas with the disc galaxy (t = 2–4).

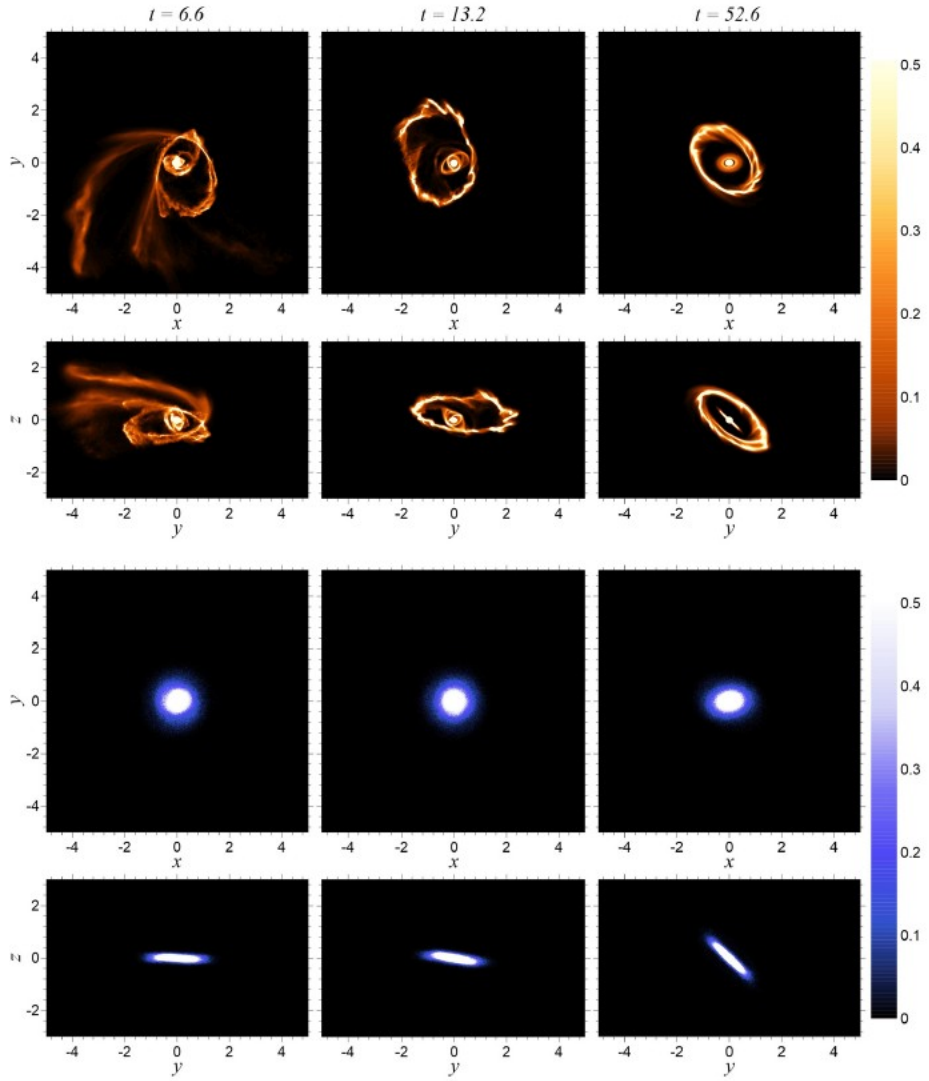

Figure 3: Surface density distributions of the gaseous (orange colour at the top) and stellar (blue colour at the bottom) components in various projections (XY and YZ) at the stage of formation of a new gaseous disc with opposite rotation in the precessing disc system (t = 6.6–52.6).

Simulation Results: Integral Characteristics

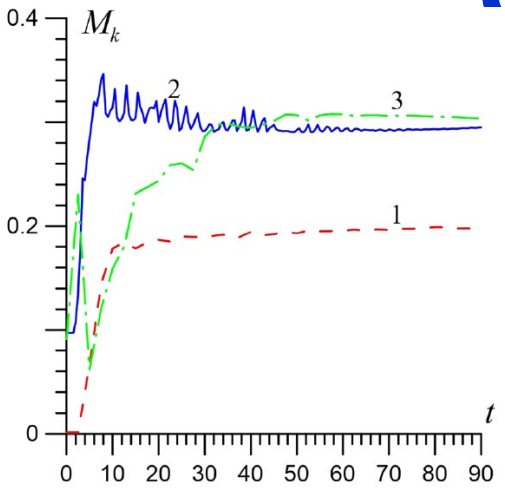

Figure 4: The evolution of the gas mass in the galactic centre M_{core} ($r < 0.1$, red line 1), in the disc M_{disc} ($r < 1$, blue line 2) and in the ring M_{ring} ($1 < r < 2$, green line 3) for the model with the retrograde gas and $\Theta_g = 20°$.

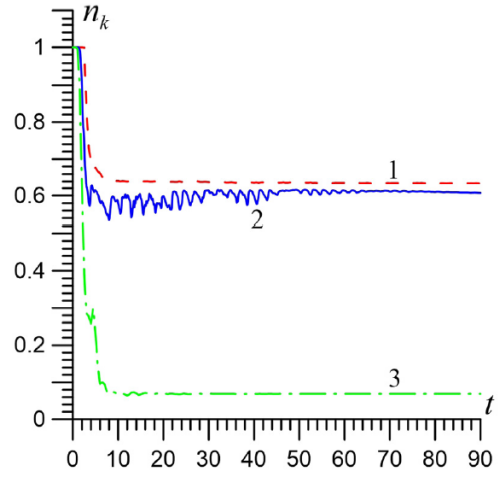

Figure 5: Dynamics of the mass fraction of the initial galactic gas in the core n_{core} ($r < 0.1$, red line 1), in the disc n_{disc} ($r < 1$, blue line 2) and in the ring n_{ring} ($1 < r < 2$, green line 3) for the retrograde gas infall model at $\Theta_g = 20°$.

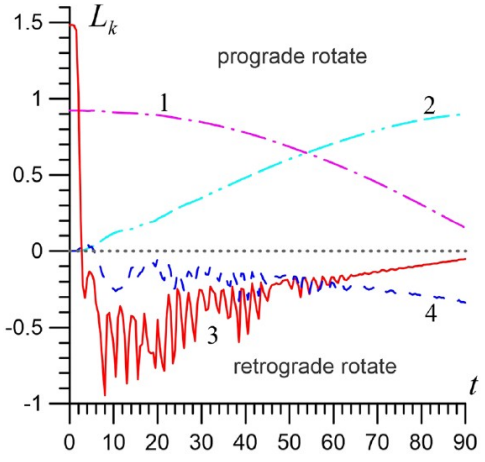

Figure 6: Evolution of the components L_z and L_y of the specific angular momentum for stellar disc (L_z, magenta line 1; L_y, light-blue line 2) and gaseous disc (L_z, red line 3; L_y, blue line 4) with $\Theta_g = 20°$.

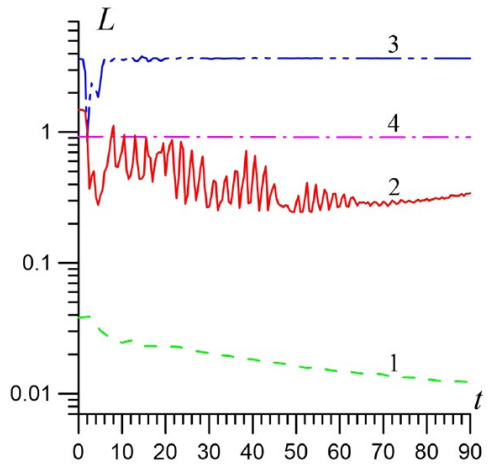

Figure 7: Specific angular momentum L *vs* time for the gas core ($r < 0.1$, green line 1), the gas disc ($r < 1$, red line 2), the gas ring ($1 < r < 2$, blue line 3) and the stellar disc ($r < 1$, magenta line 4) in the model with $\Theta_g = 20°$.

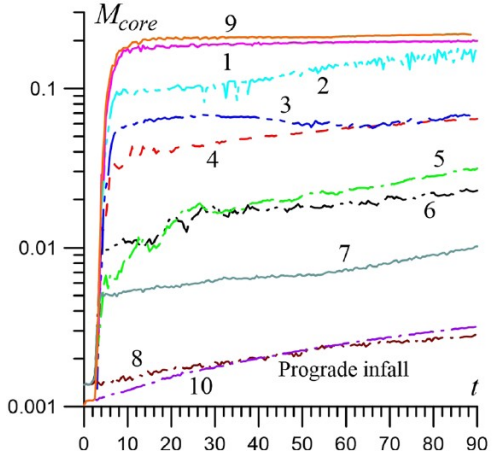

Figure 8: Influx of gas mass M_{core} into the inner region of the core ($r < 0.1$) at different angles Θ_g for retrograde infall of intergalactic gas into the disc of the bulgeless galaxy: 1 – $\Theta_g = 20°$; 2 – $\Theta_g = 10°$; 3 – $\Theta_g = 5°$; 4 – $\Theta_g = 30°$; 5 – $\Theta_g = 40°$; 6 – $\Theta_g = 45°$; 7 – $\Theta_g = 60°$. For comparison, the model with prograde infall (8 – $\Theta_g = 20°$) is also shown. Curves 9 and 10 describe galaxy models with the bulge at $\Theta_g = 20°$ for retrograde and prograde infall, respectively.

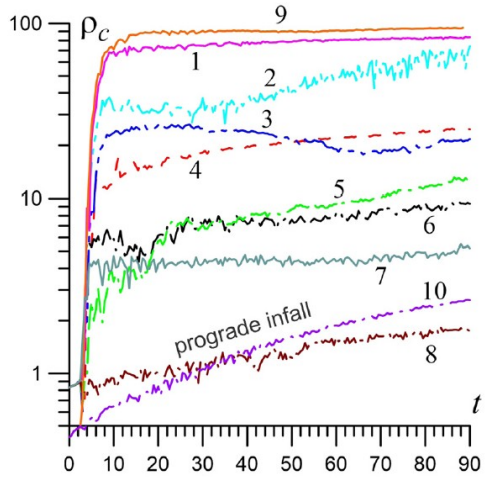

Figure 9: Evolution of the gas density in the galaxy centre ρ_c at different angles Θ_g in the model of retrograde infall of intergalactic gas. The colours, symbols, and lines are as in Figure 8.

Simulation Results: Ring

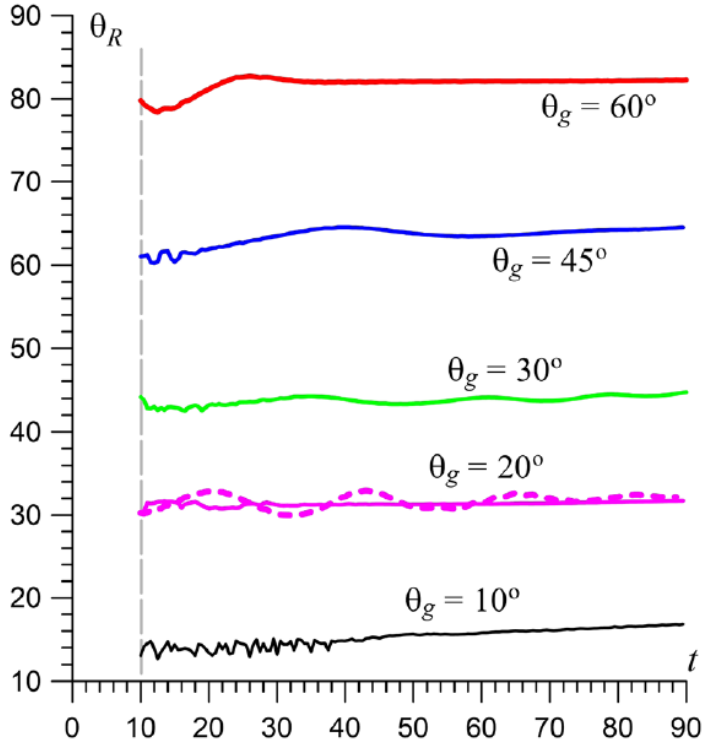

Figure 10: Dependences of the gas ring inclination angle (Θ_R) on time. The dashed line describes the behaviour of the model for $\Theta_g = 20°$ with the bulge. The vertical grey line at $t = 10$ approximately marks the end of the outer ring formation stage.

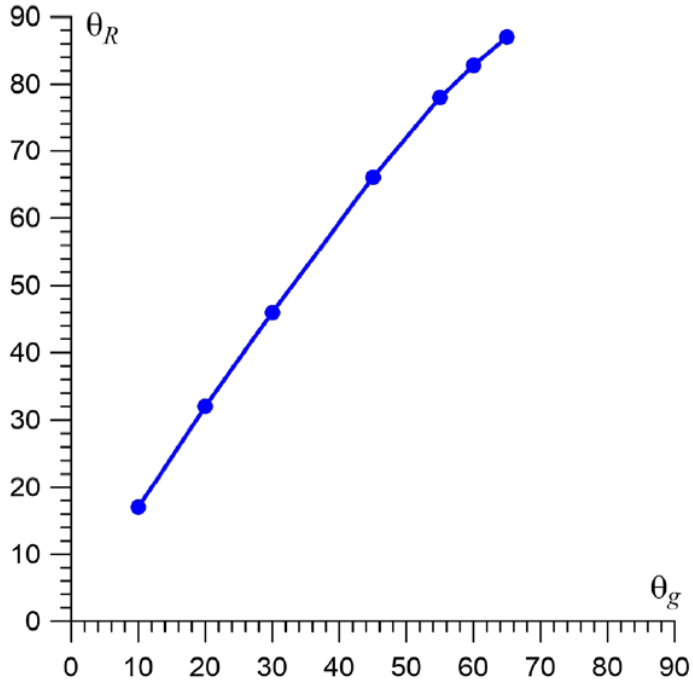

Figure 11: Relationship between the gas flow incidence angle (Θ_g) and the polar ring orientation angle at the end of the simulation (Θ_R).

Simulation Results: Collision Dynamics

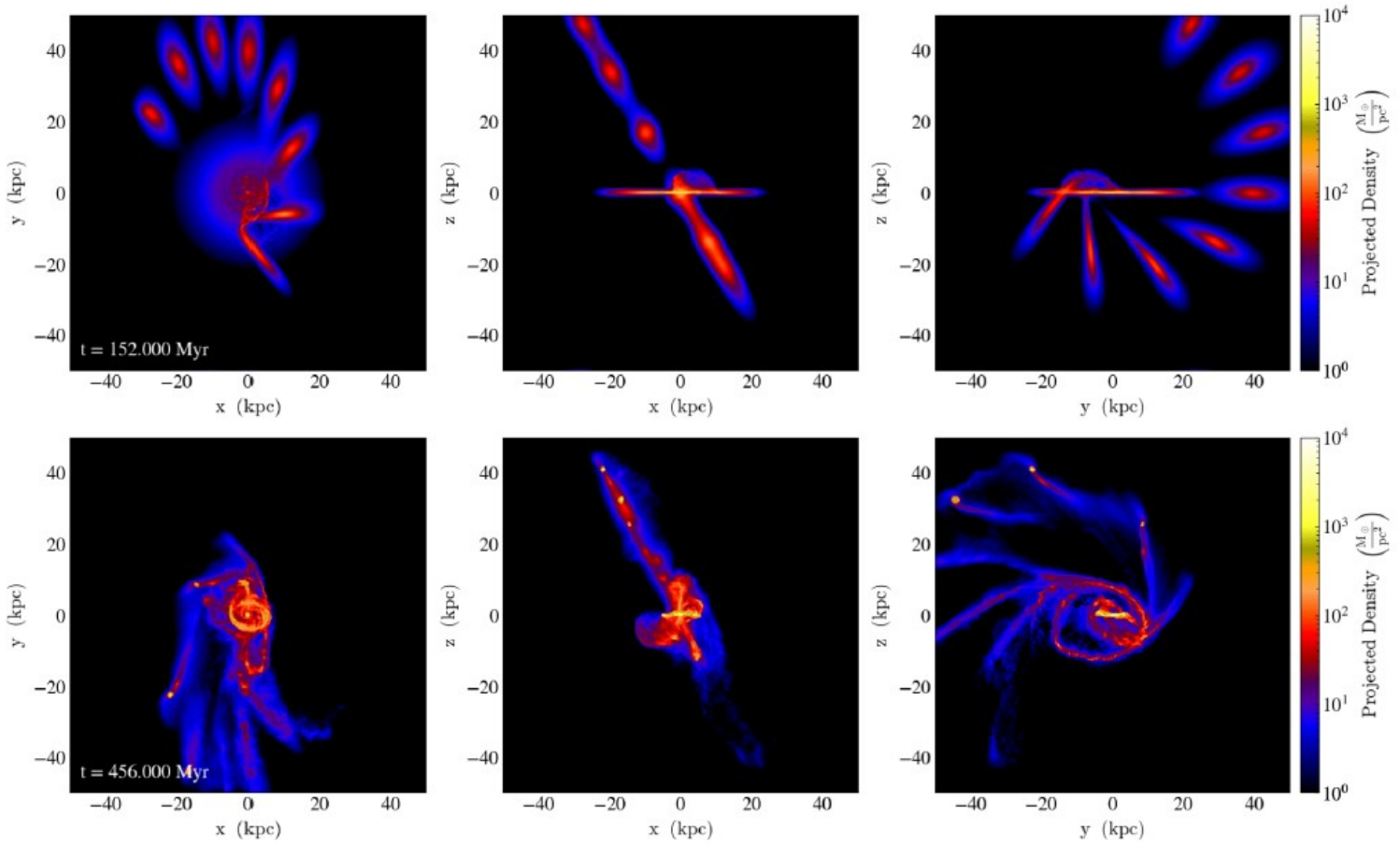

Fig. 1. Accretion of intergalactic gas onto a spiral galaxy in our numerical model. The moment of collision in the upper panel and the initial stage of polar ring formation in the lower panel (at ~ 300 Myr after the collision) are shown. Each frame has a size of 100×100 kpc along each projection (XY, XZ, YZ). The range of variation of the surface gas density along the line of sight is $1 - 10^4$ $M_\odot/pc^2$.

Simulation Results: Collision Dynamics

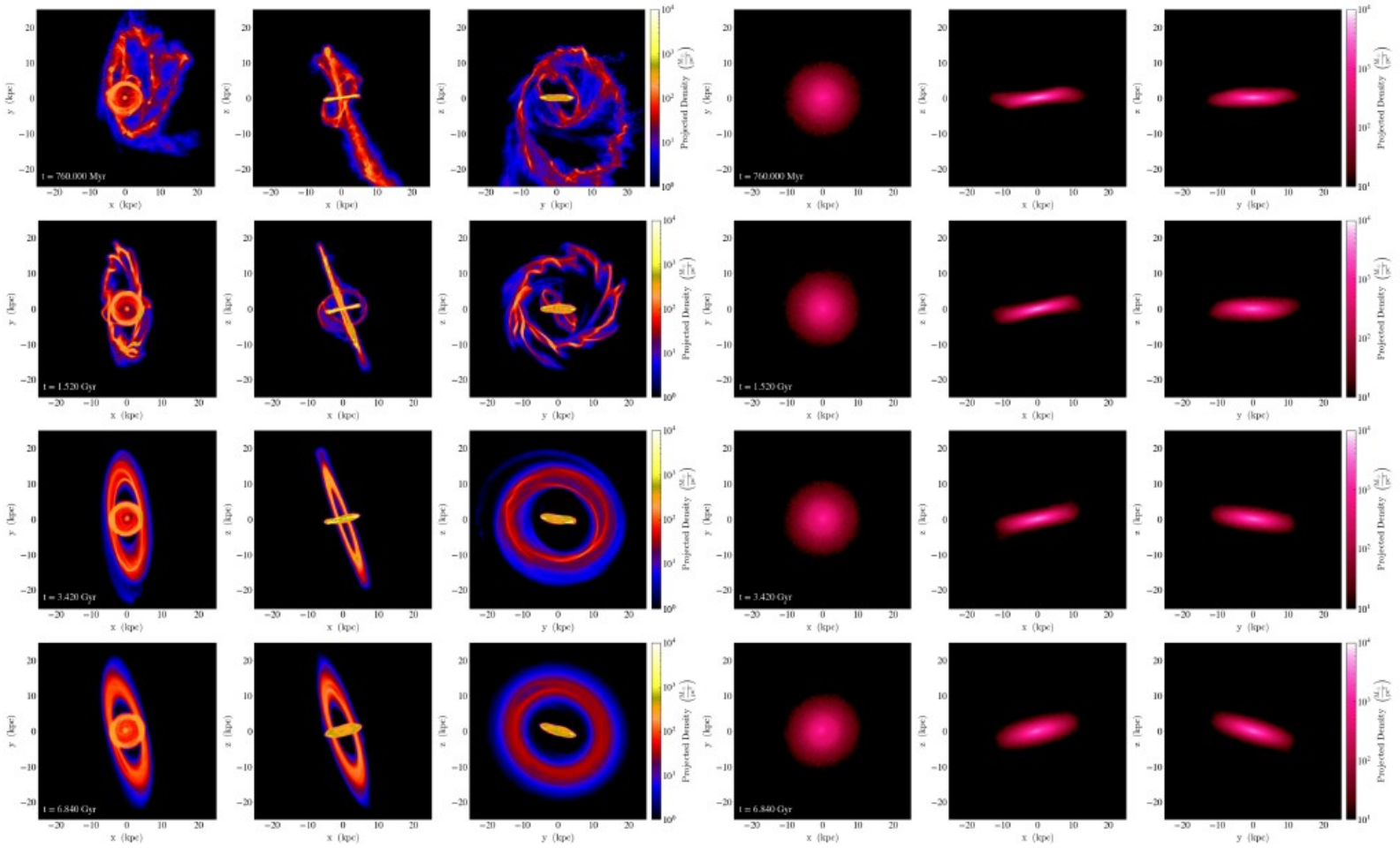

Fig. 2. Evolution of the polar gas ring in the galaxy on the time interval from 760 Myr to 6.84 Gyr. The gas subsystem of the galaxy (left) and the stellar disk (right) are shown. The frame has a size of 50×50 kpc along each of the projections (XY, XZ, YZ). The range of variation of the surface density along the line of sight of the gas is within 1–10^4 $M_\odot/pc^2$ and of the stars — $10 - 10^4$ $M_\odot/pc^2$.

Simulation Results: Collision Dynamics

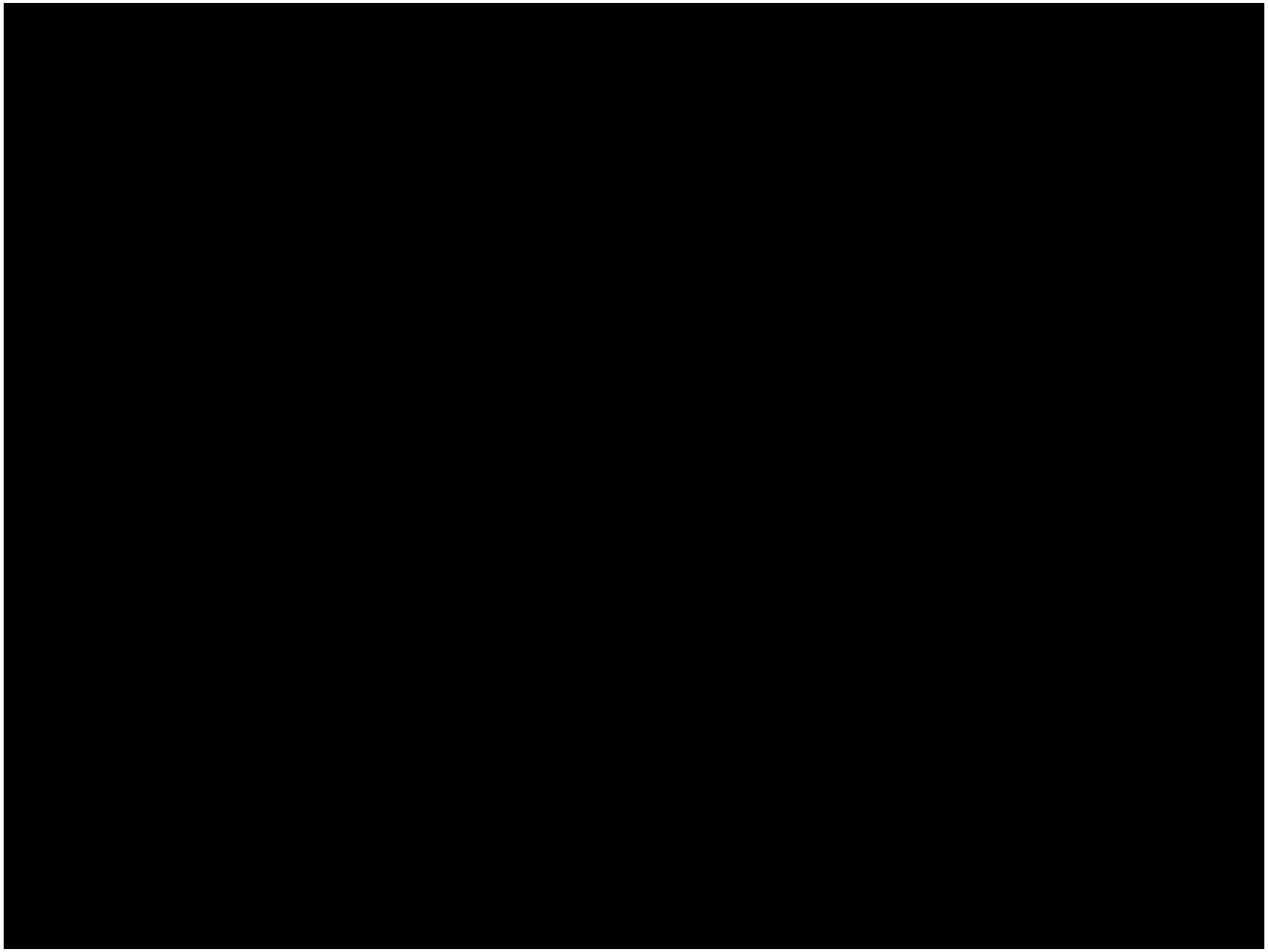

Supercomputer Simulations III

SUMMARY

We studied the dynamics of the fall of an intergalactic gas flow onto a gas-rich spiral galaxy. This accretion regime can lead to two observed phenomena simultaneously. The result is both an additional influx of gas into the region of the central supermassive black hole and the formation of outer gas rings similar to polar-ring systems.

The angle of incidence of the gas intergalactic flow onto the spiral galaxy (Θ_g) is a key parameter in our study. The efficiency of gas inflow into the AGN region is very sensitive to the angle Θ_g and is maximal at $\Theta_g \simeq 20°$. The presence of a stellar bulge in the main galaxy has little effect on the gas inflow into the central kiloparsec. The additional mass in the center of the galaxy is approximately 100 times greater in the retrograde infall of intergalactic gas compared to the prograde case. This is due to more favorable conditions for the removal of angular momentum in the gas disk.

The outer inclined gas rings are a typical result of the considered accretion of intergalactic matter at incidence angles $\Theta_g = (10-90)°$ in all numerical experiments with retrograde rotation. The angle between the outer ring and the main disk Θ_R depends on the value of Θ_g, but the condition $\Theta_R \geq 1.3 \cdot \Theta_g$ is always satisfied. The fall of gas onto the galaxy with $\Theta_g = (55-90)°$ ensures the formation of a polar ring with $\Theta_R \simeq 90°$.

Thank you!

khrapov@volsu.ru

This work supported by the Russian Science Foundation (grant no. 23-71- 00016, https://rscf.ru/project/23-71-00016/). The research is carried out using the equipment of the shared research facilities of HPC computing resources at Lomonosov Moscow State University.